Chapter 3

The Radio Galaxy:– 3C 293

3.1 Introduction

Studies of the neutral gas component associated with the nuclei of active galaxies are crucial to understanding the physical processes that take place in these objects. Such observations can be used to test unified models of active galaxies (e.g. evidence for dusty tori etc), to constrain possible fuelling mechanisms and as a diagnostic of the AGN/jet interaction with the ambient medium in the host galaxy. The extended neutral interstellar medium (ISM) of the host galaxy is often a sensitive diagnostic of galaxy interactions which may be linked to all classes of nuclear activity.

There have been several reviews that have investigated the relationship between peculiar gas and stellar dynamics in the extra-nuclear regions of active galaxies compared with the equivalent dynamics seen in radio-quiet, non-'active' galaxies (see Martel et al. 1999; Heckman et al. 1983; Balick & Heckman 1982 and refs. herein). A few of these reviews have reported some correlation between irregular dynamics and galaxy activity, although others have found little or no evidence for such conclusions. The presence of such a disturbed dynamical system is regularly considered a signature of a past galactic interaction or merger event and is often cited as a method by which material can be injected into the centre of a galaxy, losing its angular momentum and feeding the active nucleus or starburst activity.

At present the majority of MERLIN HI absorption studies have involved Seyfert and starburst galaxies (e.g. NGC 4151 – Mundell et al. 1995; M82 – Wills et al. 1998) with this method being only applied on a few occasions to more radio luminous objects (radio galaxies) such as 3C 305 (Cole 1999, Jackson et al. submitted). Neutral hydrogen has been studied via absorption in an ever increasing number of radio galaxy at either arcsecond resolution with instruments such as the VLA or WSRT (e.g. sample – Morganti et al. 2001a; Cygnus A, – Conway & Blanco 1995; Hydra A – Dwarakantha, Owen & van Gorkom 1995). Also an increasing number have been studied using VLBI HI observations (e.g. NGC 4261 – van Langevelde et al. 2000; PKS 2322-123 – Taylor et al. 1999b) but these still number only a few, with the majority of the highest resolution observations concentrating on absorption against the radio galaxy core region and resolving away any extended radio background source.

In this chapter a comprehensive study of the neutral hydrogen absorption properties of the peculiarly disturbed radio galaxy 3C 293 with $\sim 0\farcs2$ angular resolution using MERLIN will be presented. These MERLIN observations will be compared to similar resolution archival *HST* data and previously published CO and radio polarisation observations. This investigation comprises only the second detailed HI absorption study so far made using MERLIN of a radio galaxy.

3.1.1 Background – 3C 293

3C 293 is a moderately large radio galaxy with a steep-spectrum core at a redshift of $\sim$0.045; for H_0=75 km s^{-1} Mpc^{-1} its distance is D=180 Mpc and $1''$=815 pc. It

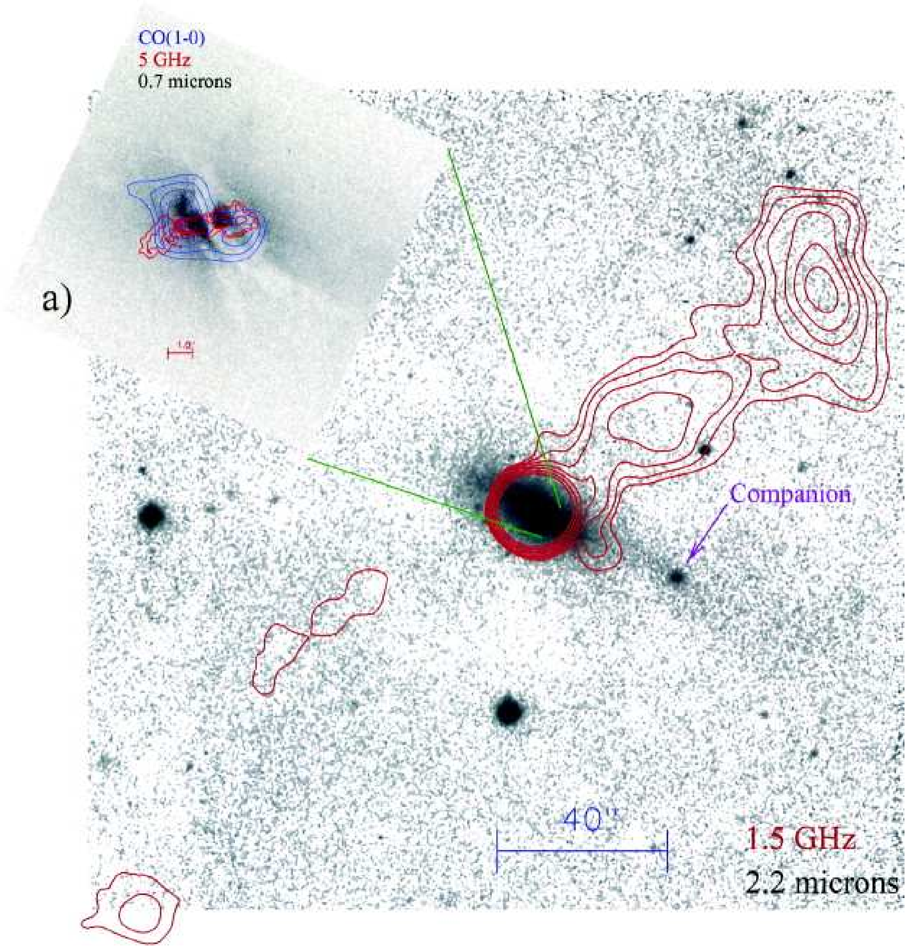

Figure 3.1: Montage of optical, radio and molecular emission from 3C 293, reproduction of figure 4 from Evans et al. (1999).

is associated with a peculiar elliptical galaxy, VV5-33-12, which contains extensive dust lanes (Battistini et al. 1980). These filamentary dust lanes are clearly observed in *HST* images to wind and split as they cross the central region of the source at a P.A. of $\sim35°$ (Martel et al. 1999). Wider field optical images show a nearby companion galaxy $\sim37''$ ($\sim$30 kpc) away (Heckman et al. 1986; Heckman, Armus & Miley 1987; Evans et al. 1999).

Recent mm-wavelength detections of CO emission and absorption (Evans et al. 1999) have inferred the presence of an asymmetric disc of molecular gas that is

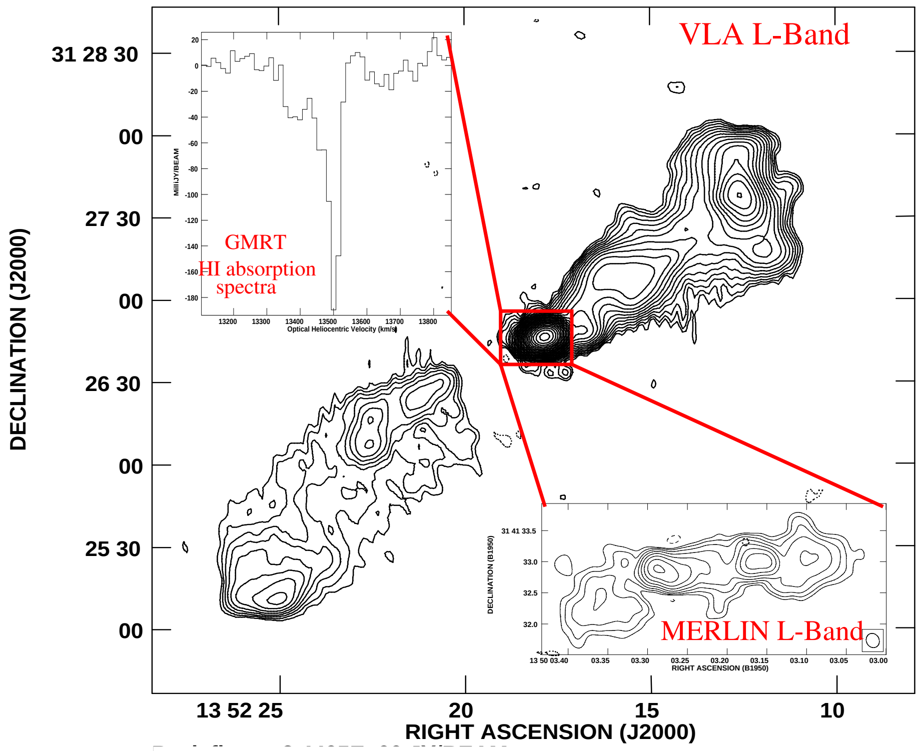

Figure 3.2: Low resolution, VLA B-configuration, 1.36 GHz map of 3C 293 with GMRT HI absorption spectra and MERLIN 1.36 GHz contour image inset. Contour levels of the main image are -1, 1, 1.414, 2, 2.828, 4, 5.657, 8, 11.31, 16, 22.63,32, 45.25, 64, 90.51, 128, 181.0, 256, 362, 724.1, 1020, 1450, 2050, 2900, 4100, 5790 $\times 0.5$ mJy beam^{-1}. GMRT spectra is plotted as absorbed flux density in mJy beam^{-1} versus optical heliocentric velocity in km s^{-1} and has a velocity resolution of 13.2 km s^{-1}. Inset MERLIN image is identical to that presented in Fig. 3.4. Main VLA image is courtesy of G. B. Taylor.

apparently rotating around a compact core. These observations have confirmed that there is a high concentration of molecular gas within the central few kiloparsecs of this radio galaxy (see for example Figure 4 of Evans et al. – reproduced as Fig. 3.1, which clearly shows concentrations of CO within the centre of 3C 293 along with optical images of the galaxy and it's companion) lending considerable support to the idea that this galaxy has recently been involved in a gas-rich galaxy-galaxy interaction in which large volumes of gas and material have been cannibalised and are now being used as fuel for this AGN.

At high angular resolution the steep spectrum radio core component is resolved into two luminous components separated by $\sim 2''$ each of which appear to further resolve into several more compact radio sources (see Fig. 3.3; Bridle, Fomalont & Cornwell 1981; Akujor et al. 1996). Adjacent to each of these compact radio components are less luminous lobe-like structures seen in 1.4 GHz sub-arcsecond resolution radio images. At lower resolution, a large-scale 'Z-shaped' radio structure extending from this central steep spectrum core region, see Fig. 3.1 & 3.2 (Bridle et al. 1981; Evans et al. 1999). The large scale radio jets themselves point almost perpendicular to the complex set of dust lanes that are so distinctive in the high resolution optical images.

Neutral hydrogen absorption has previously been detected in 3C 293 both with single dish observations (Baan & Haschick 1981), WSRT (Shostak et al. 1983) and studied in detail using the early VLA at A-configuration with a reduced number of telescopes (Haschick & Baan 1985).

3.2 Observations and Image Processing

3.2.1 MERLIN

The radio galaxy 3C 293 was observed with the MERLIN array (Thomasson 1986) of 7 telescopes at 1359 MHz on April 8$^{\rm th}$ 1998. Both left and right hands of circular polarisation were measured each with 8-MHz bandwidth. The data were then correlated into 64 channels in frequency each with a bandwidth of 125-kHz, resulting in a velocity resolution of $26.3\,{\rm km\,s^{-1}}$. Frequency channel 32 was centred upon the optical-heliocentric velocity for 3C 293 ($13\,500\,{\rm km\,s^{-1}}$).

The observations were made over a period of 18 hours regularly interspersed with observations of OQ208 which was used for phase calibration. OQ208 was also

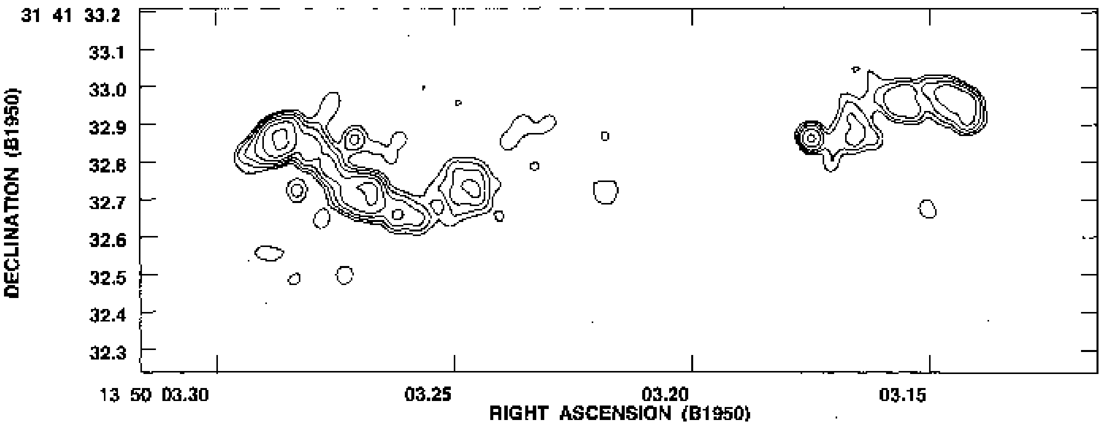

Figure 3.3: MERLIN 5 GHz continuum image of the central few kiloparsecs of 3C 293, reproduced from Akujor et al. (1996). The contour levels are 1, 2, 4, 8, 16 and 32 mJy beam^{-1}, the image has been restored with circular 50 mas Gaussian beam.

strong enough (0.7 Jy) to be used for bandpass calibration. An observation of 3C 286 at either end of the run of observations was used to calibrate the absolute flux density scale. This was achieved by assuming that 3C 286 has a flux density of 15.05 Jy at 1359 MHz (Baars et al. 1977). All initial editing and calibration was carried out using standard MERLIN software routines.

The data were further reduced and edited within AIPS where further phase corrections were derived via self-calibration methods. The data were subsequently Fourier-transformed using the AIPS task HORUS to create both uniformly and naturally weighted spectral line data cubes. Preliminary assessment of the data revealed that channels 45-55, towards one end of the observed band, were strongly contaminated with interference (see Fig. 2.7). The channels containing interference and HI absorption were well separated in frequency allowing the simple editing of the radio frequency interference without affecting the HI absorption. This conclusion was independently checked by creating a spectral cube of OQ208, which allowed the extent and position of the interference to be established. Continuum images were formed from both the natural and uniformly weighted data cubes by combining 28 channels that were free from line and interference signals. These continuum images were subsequently subtracted from the appropriate data cubes to produce continuum-subtracted spectral-line cubes. The resulting spectral-line cubes and continuum data were deconvolved using a CLEAN based algorithm (Högbom 1974) to remove instrumental response. The cleaned continuum data and continuum-subtracted spectral-line cubes were then recombined allowing specific spectra to be extracted and further spectral-line analysis to be carried out.

3.2.2 GMRT

In addition to these MERLIN observations, 3C 293 was also observed using the GMRT, (Swarup et al. 1991) on November 12th 2000 for 10 hours. During the observations between 24 and 27 of the 30 available, 45 m diameter, telescopes of the GMRT were used at anyone time with various telescopes being lost from the experiment due to scheduled engineering work. These observations were made in both hands of circular polarisation across an 8-MHz bandwidth and correlated into 128 spectral line channels with a resulting velocity resolution of 13.2 km s^{-1}. The 64th channel was tuned to coincide with the redshifted HI line in 3C 293 at a optical-heliocentric velocity of 13 500 km s^{-1}. Observations of the phase calibration source 1347+122 were regularly interspersed with those of the source. 1347+122 was also used as a bandpass calibration source in this experiment. Two observations of 3C 286, made at either end of the run, were used to calibrate the flux density scale.

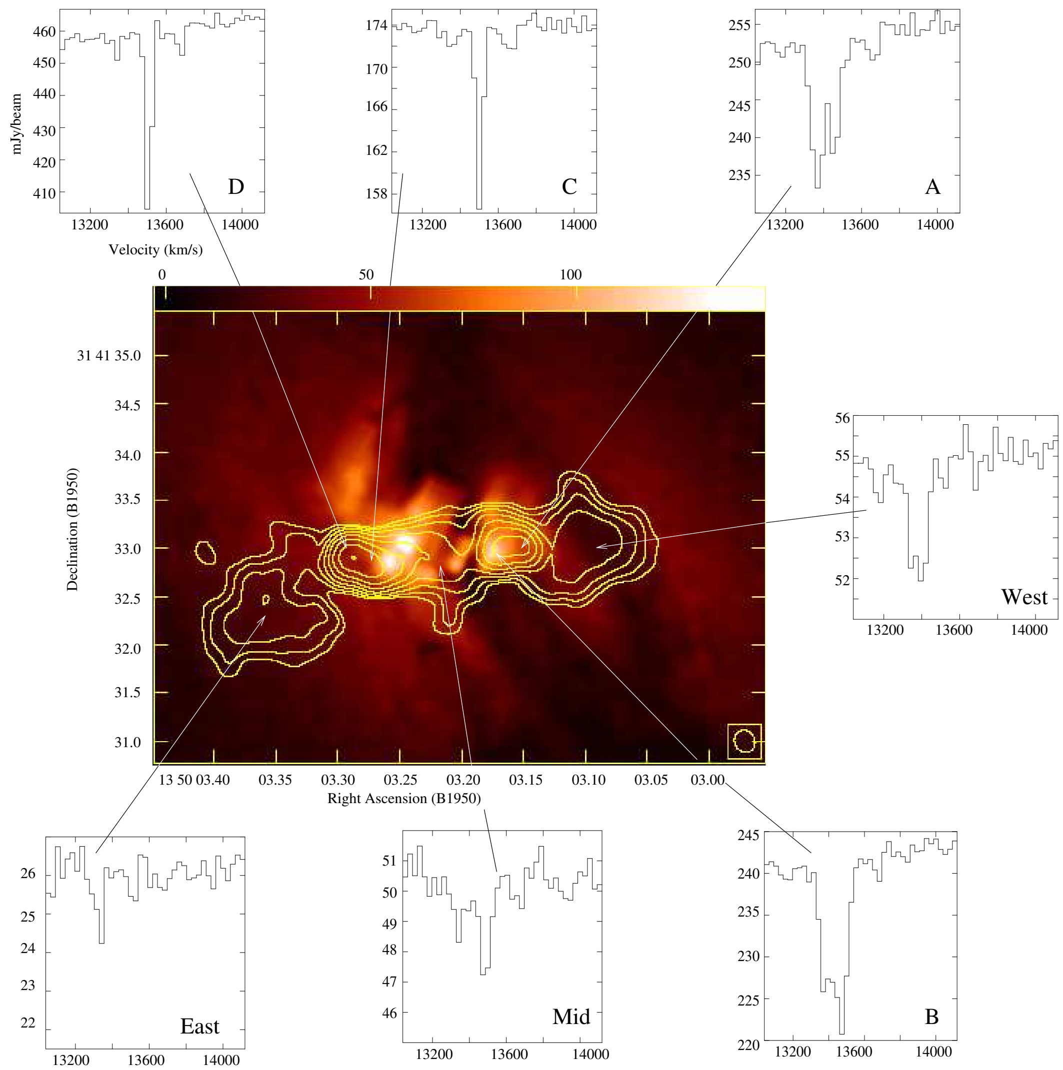

Figure 3.4: A montage showing a 1.36 GHz naturally weighted continuum map of the central region of 3C 293 with selected absorption spectra superimposed. The background image shows a false-colour *HST* image of 3C 293. The two images are astrometrically aligned to accuracy of better than 0.3 acrseconds. The angular resolution of the image is 0.235×0.205 arcseconds and contour levels are set at -3, 3, 6, 12, 24, 48, 96, 192, and 384 × 1.5 mJy beam^{-1}. The spectra are plotted with flux density in mJy beam^{-1} against velocity in km s^{-1}.

3.2.3 HST

An archival *HST* WFPC-2 snapshot image was obtained and used as a comparative image to the MERLIN radio maps. The *HST* data (ID No: U27I5A01A) were reduced using STSDAS and STARLINK software then imported into AIPS for further imaging and comparison to the radio data. The 280 second *HST* WFPC-2 exposure was taken with a broadband (*F702W*, approximates to *Cousins R-Band*) filter which includes significant levels of contaminating Hα and [N II] $\lambda\lambda$ 6548, 6583Å line emission at the redshift of 3C 293. This filter was specifically chosen by the proposer to produce snapshot images that were sensitive to morphological features such as dust lanes.

The task of aligning the *HST* data with the radio images involved initially placing a coordinate frame upon the *HST* image. This was achieved by assigning the observed positions of six stars in the WFPC-2 field with coordinates derived from the USNO star catalogue. The stars used were well spread across the WFPC-2 field enabling the curvature of the coordinate frame to be well accounted for across the majority of the relevant area of optical image. The positional error in the alignment of the final radio and optical fields shown in Fig. 3.6 is estimated to be no more than 0.3 arcseconds.

3.3 Results

The structure of the HI absorption against the central three kiloparsecs of 3C 293 is shown in a preliminary spectrum (see inset within Fig. 3.2) produced from the observations using the GMRT. The velocity resolution of these observations is a factor of two greater than those made with MERLIN. This spectrum has been extracted from a continuum subtracted cube with an angular resolution of $2''.75 \times 1''.90$.

Component	R.A.	Dec.	$S_{1.36GHz}$
	13^h50^m	$31°41'$	(Jy)
East	$3^s.36$	$32''.3$	0.56
D	3.29	32.9	0.97
C	3.27	32.8	0.62
Mid	3.21	32.6	1.24
B	3.17	33.0	1.82
A	3.15	33.0	0.73
West	3.10	33.1	0.55

Table 3.1: Summary of radio continuum properties for the central region of 3C 293.

The MERLIN naturally and uniformly weighted continuum maps are shown in Figs. 3.4 & 3.5. The angular resolution and noise levels for the naturally weighted image is $0''.23 \times 0''.21$ and 0.2 mJy beam^{-1} whilst in the uniform image they are $0''.18 \times 0''.16$ and $\sim$0.3 mJy beam^{-1}. The channel based noise level of the naturally weighted cube is 0.8 mJy beam^{-1}. A selection of line plus continuum spectra taken from the indicated regions of continuum emission are displayed in Fig. 3.4. These spectra show that absorption is apparent over most of the central few kiloparsecs. Individual continuum features are labelled in Figs. 3.4 & 3.5, following and extending the convention employed by Bridle et al., (1981). The line and continuum properties of these components are shown in Table 3.1 & 3.2. Positions of each of the components were obtained by Gaussian fitting to the peaks in the image, and line properties – central velocity and velocity width (FWHM) – were produced by fitting one or two component Gaussian models to the individual spectra. The optical depths and column densities quoted were calculated directly from the absorption spectra using $N_H = 1.823 \times 10^{20} \int \tau dV$, assuming an electron spin temperature of 100 K. The estimated optical extinction coefficient, A_B, is also calculated from the neutral hydrogen column densities using $A_B = 8.62 \times 10^{-22} N_H$ mag. derived from galactic gas-to-dust ratios (Staveley-Smith & Davies 1987).

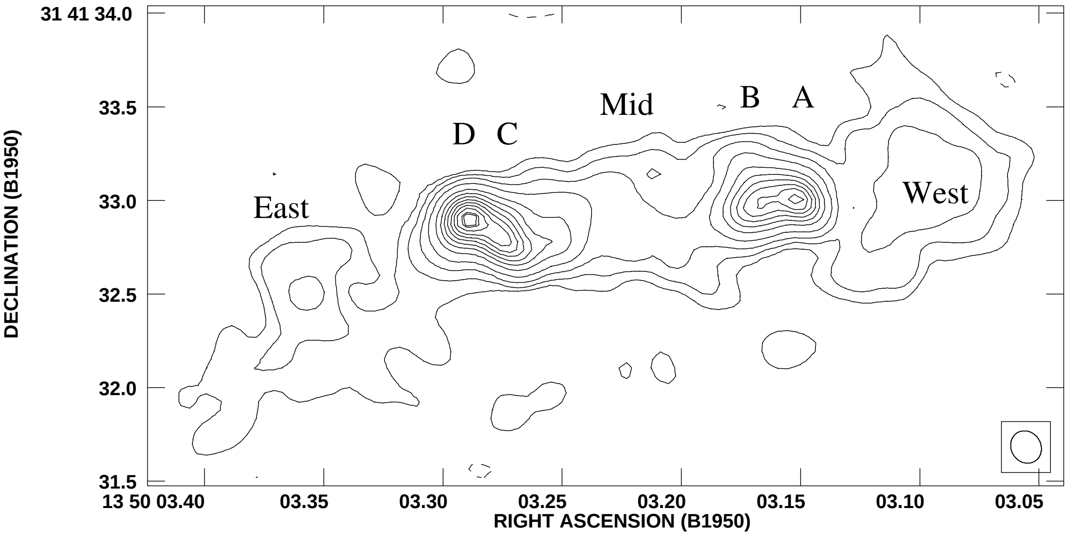

Figure 3.5: A 1.36 GHz uniformly weighted continuum map of the central region of 3C 293. The angular resolution of the image is 0.178 $\times$ 0.159 arcsec and contour levels are set at -2, 2, 4, 8, 16, 32, 48, 64, 80, 96, 112, 128, 144 and 160 $\times$ 6 mJy beam^{-1}.

Both continuum images show two strong radio components (labelled in Fig. 3.4; AB and CD), these are separated by a 1.5 arcsecond and each can be seen to be made up of two further components. These four components are resolved in Figs. 3.4 & 3.5 and labelled A, B, C and D (from right to left). The continuum of 3C 293 on large scales has been described as having a 'Z-shaped' morphology (Bridle et al. 1981) but this is not evident on the scale and resolution of these images. At the resolution of MERLIN at 22 cm ($\sim 0\rlap{.}''2$) the continuum structure of 3C 293 is roughly east-west with a position angle of $\sim$95°. The continuum images shown in Figs. 3.4 & 3.5 are consistent with similar resolution maps previously published at 1.7 GHz (MERLIN) and 8.4 GHz (VLA A-array) (Bridle et al. 1981; Akujor et al. 1996). Akujor et al. (1996) concluded that the inverted spectral index and unpolarised nature of radio component B implies that it represents the nucleus of 3C 293, as had previously been suspected by van Breugel et al. (1984). In these 1.4 GHz observations B is amongst the brightest

Component[1]	Velocity (V_c)[2] km s^{-1}	Velocity Width (Δv)[2] km s^{-1}	τ	$\int \tau$dv	N_H $\times 10^{21}$ atoms cm^{-2}	A_B mag
East	13336	42	0.069	2.90	0.53	0.46
D	13505	39	0.147	5.73	1.05	0.91
C	13504	40	0.155	6.20	1.13	0.97
Mid	13487	46	0.075	3.45	0.63	0.54
B	13380, 13470	59, 74	0.082	9.69	1.77	1.53
A	13366, 13458	74, 54	0.082	9.25	1.69	1.46
West	13378	81	0.074	5.99	1.09	0.94

Table 3.2: Summary of HI absorption properties & dust extinction estimates for the central region of 3C 293. Column densities for individual components have been calculated using $N_H = 1.823 \times 10^{20} \int \tau dV$, and assuming a spin temperature of 100 K and has been extrapolated into blue optical extinction coefficients, A_B via galactic dust-to-gas ratios using $A_B = 8.62 \times 10^{-22} N_H$ mag.

of the observed components.

Figure 3.6 (upper frame) show an inverse grey-scale representation of the extent and optical depth of the absorbing HI gas within the centre of 3C 293. Running approximately north-south across this image there are distinct stripes of increased optical depth (areas of lighter grey-scale). To enable a direct comparison between radio and optical results to be made, the MERLIN naturally weighted image is overlayed as contours on the optical WFPC-2 image in Fig. 3.6 (lower frame). By comparing the two frames shown in Figs. 3.6 it can be seen that the location of the stripes of highest optical depth of HI correlate exactly with the positions of the strong dust lanes that run through the *HST* image.

Contour maps of single channels of the continuum-subtracted cube (Fig. 3.7) show

[1] Labels are shown in Fig. 3.4 and follow and extend the convention used by Bridle et al. (1981). It should be noted that these components refer to the position that the spectra were taken and not the individual absorption line components which the labelling system employed by Haschick & Baan (1985) refers to.

[2] For A and B a two component Gaussian model was used. In these cases two values of V_c and Δv are given. For these components the $\int \tau$dv and N_H were calculated by summing the values for each individual line component.

absorption over nine channels ($\sim$240 km s^{-1} in total). The absorption against component CD is narrow, FWHM$\approx$40 km s^{-1} (see spectra in Fig. 3.4) with just one spectral component visible at this velocity resolution. Towards the continuum feature AB broad, multiple spectral component absorption is detected compared with narrower absorption detected against other areas of the source.

Figure 3.8 shows a position-velocity diagrams as a function of Right Ascension. Figure 3.8a shows as contours the absorbed flux density while Fig. 3.8b shows the opacity.

3.4 Discussion

3.4.1 Comparison of MERLIN (atomic hydrogen), HST (dust) and Molecular Gas (CO emission and absorption)

3C 293 is clearly a very gas rich radio galaxy with some degree of tidal distortion. In the broadband optical *HST* image extensive, distorted dust lanes crossing the central region of the galaxy. Considerable quantities of neutral gas, HI, and molecular, CO, (Evans et al. 1999) have been detected in the central few kpc of 3C 293. Evans et al. have inferred a molecular gas mass of 1.5×10^{10} M$_\odot$ using standard CO-to-H$_2$ mass conversion factors they infer a H$_2$ column density of $\sim$530 M$_\odot$ pc^{-2} within the inner 3 kpc. The molecular column density that Evans et al. derive for the inner region of 3C 293 is approximately one tenth of the HI column densities calculated, from this data, using an assumed spin temperature of 100 K.

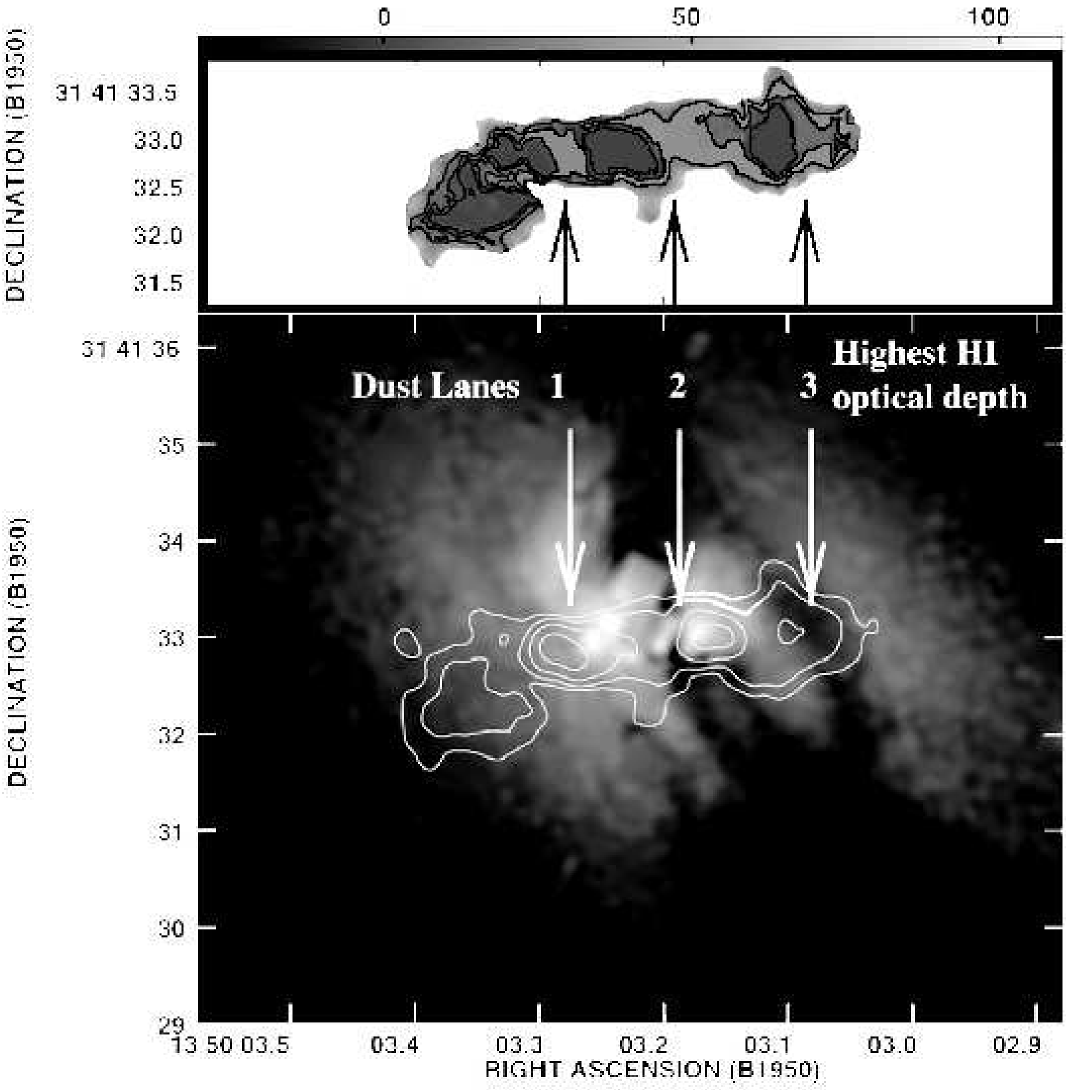

Figure 3.6: (Upper-panel) Grey-scale and overlayed contour map of total optical depth integrated over the velocity range 13300→13550 km s^{-1}. The grey-scale is negative (lightest areas represent highest optical depth). (Lower-panel) Grey-scale *HST* WFPC-2 image of 3C 293 overlayed with the naturally weighted MERLIN continuum map.

The integrated optical depth over the velocity range (13 200→14 000 km s^{-1}) of HI absorption (Fig. 3.6) shows that the areas of highest HI optical depth are co-spatial with the multiple dust lanes found towards the centre of 3C 293. By assuming standard galactic gas-to-dust ratios it is possible to derive a blue optical extinction coefficient, A_B, from the neutral hydrogen column densities (see Table 3.2). Across the areas of highest HI column density the calculated optical extinction is ∼1.5 mag. This value is comparable to the extinction seen in Fig. 3.6 which is estimated to vary between 0.7→2.1 magnitudes across the most obscuring dust lanes. It should be noted that the extinction values calculated from the optical images are rough estimates, derived by assuming that the apparent brightness in the areas obscured by the dust lane should be equal the observed brightness adjacent to these dust lanes.

3.4.2 Broad and Narrow HI Absorption Spectral Components

The HI absorption structure observed against 3C 293 can be split into two categories; those with narrow velocity widths (<50 km s^{-1}, centred at velocity ∼13 500 km s^{-1}) and those with broad velocity widths (>65 km s^{-1}) seen against the western half of the source (see Fig. 3.4). In addition an extended constant velocity component is visible in Fig. 3.8 at ∼13 325 km s^{-1}, although this component will not be discussed in detail it is considered to be a real (rather than a bandpass effect or interference) since it is apparent in the spectra shown in Fig. 3.4 and it is consistent in both velocity and position with spectral component 10 observed by Haschick & Baan (1985).

In the following sections the distribution and kinematics of the neutral gas component will be discussed. Firstly a brief explanation of the origin and velocity structure of the main (13 500 km s^{-1}) narrow HI absorption will be given. Fol-

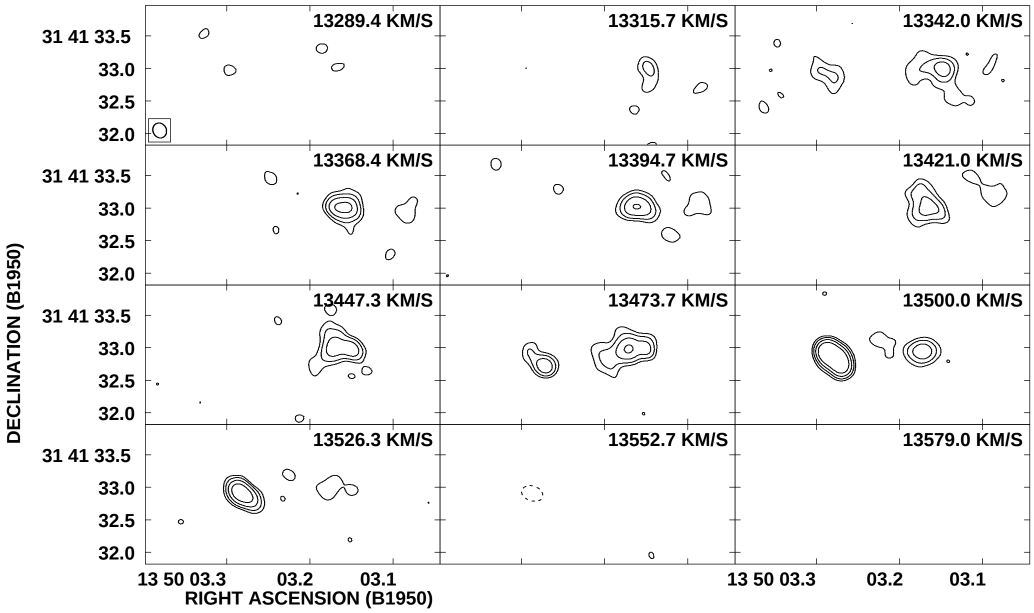

Figure 3.7: Contour maps of individual channels in the naturally weighted continuum subtracted spectral line cube. The contour levels are -32, -16, -8, -4 and 4 mJy beam^{-1}, and the velocity that each channel is centred upon is labelled on each panel.

lowed by a discussion of the broad absorption components along with implications for the orientation of the radio source with respect to the neutral gas.

Narrow HI Absorption

Although the narrow velocity HI absorption component is predominantly observed against the eastern half of the radio continuum source, it may also be present in the spectra against the western part of the source but not easily visible in the presence of the strong broad velocity absorption components. This component is consistent in velocity and line width with the narrow CO absorption components observed by Evans et al. (1999). The narrow absorption can be interpreted as the result of quiescent gas at some distance from the centre of the galaxy, similar to the HI absorption features observed in other disturbed galaxies (Mrk 273, Cole

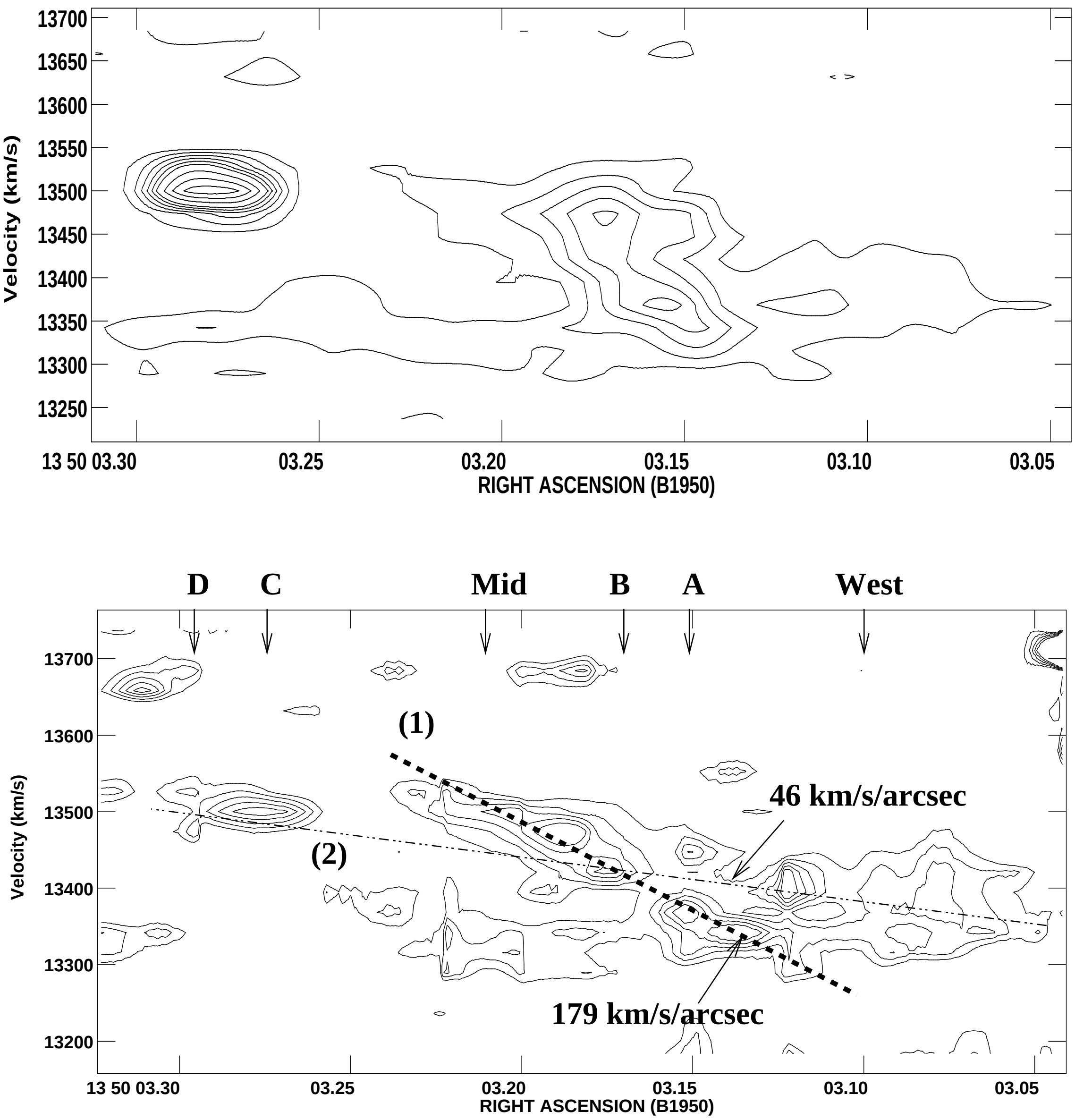

Figure 3.8: a) (Upper-panel) Right Ascension vs. Velocity plot across the central region of 3C 293 at declination 31° 41′ 32.″0. The contour levels are -20, -18, -16, -14, -12, -10, -8, -6, -5, -4, -3, -2,-1 and 1 mJy beam^{-1}. b) (lower-panel) Right Ascension vs. Velocity contour map produced by combining optical depth values in declination across the source. The contour levels are τ equal to 0.06, 0.09, 0.12, 0.15 and 0.18. It should be noted that the errors in the calculated optical depth of HI vary across this image and are significantly greater against areas where less continuum flux density is observed. As a result comparison with the upper panel (absorbed flux density) should be made to asses the reality of features.

et al. 1999).

In 3C 293 the narrow velocity HI absorption component is observed to have a small associated velocity gradient (see Fig. 3.8b) of $\sim$46 km s^{-1} arcsec^{-1}. This velocity gradient is consistent with gradients of $\sim$40 km s^{-1} arcsec^{-1} seen in optical emission lines (van Breugel et al. 1984) that stretch out to a radius of 10 kpc from the nuclear region. Assuming that the neutral and ionised gas producing these two velocity gradients are associated implies that the neutral gas producing the narrow velocity absorption component is situated up to $\sim$10 kpc away from the core region. Considering this, it is likely that the observed velocity gradient is the result of bulk rotational motions of gas in the galaxy, implying an enclosed mass of $M(< 9\ \mathrm{kpc}) \approx 2 \times 10^{11}\ M_\odot$. This enclosed mass is consistent with the binding mass derived by van Breugel et al. (1984).

Broad HI Absorption

The broad, complex absorption observed against the western side of 3C 293, especially components AB, can be explained by the assumption that the neutral gas is in a more turbulent state in front of these areas of the radio continuum. This is not surprising if the location of the central engine of this radio galaxy is assumed to be co-spatial with the radio nucleus – component B (see Fig. 3.3 & 3.4). Association with the active nucleus could result in gas clouds moving with line of sight velocity different from the ambient velocity of the galaxy. The resultant velocity dispersion could account for the observed broad absorption lines. The origin of this disturbance is likely to be due to infall and outflow of gas from the core but the existence of a rotating gas disc near to the AGN, as has been suggested by van Breugel et al. (1984), Haschick & Baan (1985) and Evans et al. (1999), could also create the observed broad line widths.

3.4.3 Comparison of Depolarisation of the Radio Continuum and HI Absorption

To better understand this source we can use the fact that the absorbing gas must lie in front of the radio continuum. This allows some constraints to be placed upon the position of the radio structure relative to the gas in the system. The column densities of HI (see Table 3.2) observed against the continuum components on the western side of the radio structure are systematically higher than those seen against the eastern components implying more neutral hydrogen is present along the line-of-sight of the western radio continuum components.

As well as the neutral gas having higher column densities in front of the western half of the source, there is strong evidence from polarisation measurements that the ionised gas component is also higher in front of this region. At 8-GHz Akujor et al. (1996) have observed that the western components are considerably more depolarised than their eastern counterparts. This asymmetry in depolarisation decreases with higher frequency observations. These polarisation properties of a radio source are typically associated with the effects of an intervening region of ionised gas that radio emission must pass through (i.e. The Laing-Garrington effect, Laing 1988; Garrington et al. 1988). This result can be interpreted either as evidence that the neutral/ionised gas is localised around the radio core (B), or that the eastern components are in front of a more extensive region of gas.

3.4.4 Gas Dynamics in the Central kpc: A Rotating Ring of Gas?

Observations of both molecular (Evans et al. 1999) and ionised (van Breugel et al. 1984) gas show evidence of rotation across the central 10 kpc. As discussed above, evidence for this gradient is seen in the narrow velocity component,

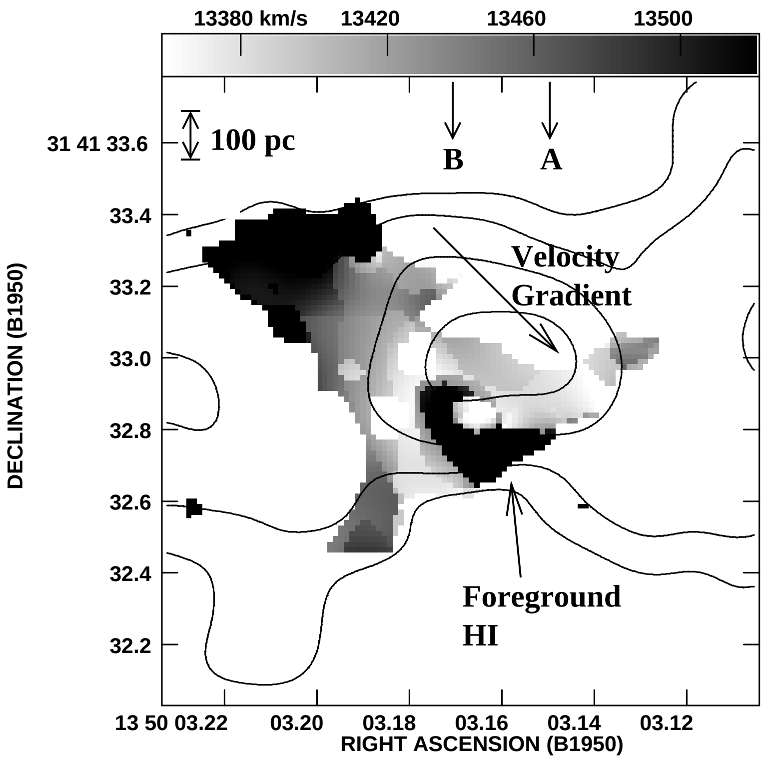

Figure 3.9: The velocity of optical depth of HI gas in front of the radio component B overlayed upon radio continuum contours. It should be noted that a clump of higher velocity (~13550 km s^{-1}) gas appears superimposed upon the velocity gradient. This spectral component has a similar velocity and width of the narrow absorption component discussed in section 3.2 and as such is considered to be a clump of high optical depth foreground gas. Areas that are not covered by the grey-scale have been blanked during the processing on the basis of signal strength present in the optical depth cube.

however the broad line absorption shows a steeper 179 km s^{-1} arcsec^{-1}, more localised gradient centred on the nuclear continuum component B (Fig. 3.8b). This localised velocity gradient can be explained by the existence of a disc of gas centred at B.

The orientation of such a disc is required to provide large column densities along the line-of-sight towards AB but not CD. This can be achieved by a near edge-on disc at an angle to the radio axis and of sufficiently small thickness so as to provide a high opacity towards B but a low opacity towards CD. This is supported by

CO line emission observations (Evans et al. 1999) which infer the existence of a gas disc. This is consistent with the HI absorption observations presented here which observe a steep velocity gradient which is centred upon radio component B (see Fig. 3.8 & 3.9) and no broad HI absorption against CD.

In Fig. 3.8 the 179 km s^{-1} arcsec^{-1} velocity gradient can be seen to extend over $\sim 1\farcs5$. This velocity gradient can be explained by a rotating, near edge-on, ring of neutral gas with an orientation similar to that of the velocity gradients observed by Evans et al. (1999) and van Breugel et al. (1984). Fig. 3.9 shows the velocity structure in the vicinity of this circumnuclear gas ring, showing a velocity gradient at a P.A. $\sim 45°$ with an extent limited by the presence of background continuum. Hence it is possible to set a lower limit on the radius of this disc of $\sim$600 pc. This orientation implies that the radio jet and the circumnuclear ring must undergo a significant shift in relative angle on scales smaller than the resolution of these observations close to the core for the jet to be emitted perpendicular to the disc. These deviations in the jet position angle are tentatively observed in the MERLIN 5 GHz image (Fig. 3.3) and are also seen in high resolution 1.4 GHz images (see chapter 7, Fig. 7.2).

Assuming the gas ring is nearly edge-on with an angle of $\sim 30° \rightarrow 45°$ between the disc and the radio axis, the mass required to bind this system would be $M_{\rm dyn}(< 600\ {\rm pc}) \leq 3.9 \times 10^{9} (\sin^{-2} i)\ M_{\odot}$, where i represents the inclination of the disc (i.e. for an edge-on disc i=90°).

In Fig. 3.8b numerous individual components of varying optical depth comprise the rotating disc. These clumps of increased opacity can be inferred to represent clouds of HI gas within a fragmented disc. Of these gas clouds, those that cover the greatest spread in velocity are predominantly positioned at a similar R.A. to the continuum component B, the position of the suspected AGN. Several of these clouds of neutral gas are spatially resolved with sizes ranging up to $\sim 0\farcs33$ (270 pc). Assuming a uniform optical depth similar to that calculated from the HI absorption spectra against component B in Fig. 3.4 these gas clouds contain a mass of HI $\leq$ few $\times 10^6$ $M_\odot$. This is consistent with the estimates of M_{cloud} $<1\times10^6$ $M_\odot$ by Haschick & Baan (1985) for larger but significantly lower optical depth HI gas clouds they observed in 3C 293.

3.5 A Model of the Distribution of Neutral Gas and Dust in the Central Region of 3C 293

From these observations and those that previously reported on by van Breugel et al. (1984), Akujor et al. (1996) and Evans et al. (1999) it is possible to formulate a picture of the gas distribution in front of the central region of 3C 293. Firstly, these MERLIN HI observations detect two distinct velocity gradients within the gas distribution of 3C 293 (see Fig. 3.8). As was discussed in the section above the 179 km s^{-1} arcsec^{-1} velocity gradient is only distributed over a kiloparsec region surrounding the AGN and is consistent with gas rotating in a circumnuclear ring of radius $\sim$600 pc. Whereas the slower moving velocity gradient (labelled 2 in Fig. 3.8) is consistent with the rotational motions observed by van Breugel et al. (1984) in ionised gas. van Breugel et al. (1984) observed this velocity gradient to extend out radius of 10 kpc from the nucleus.

Comparisons between optical extinction due to dust and the distribution of HI are strongly correlated (see Fig. 3.6). This correlation is further confirmed when the distribution of the narrow absorbing component is isolated (see Fig. 3.10) and compared to the positions of the dust lanes (see Fig. 3.6). The spatial coincidence of the dust and narrow absorbing component along with the similarity of the velocity structure of this HI component and the previously observed velocity gradients of the ionised gas infer some degree of physical association between these three components. Assuming this physical association is true, it is reasonable to

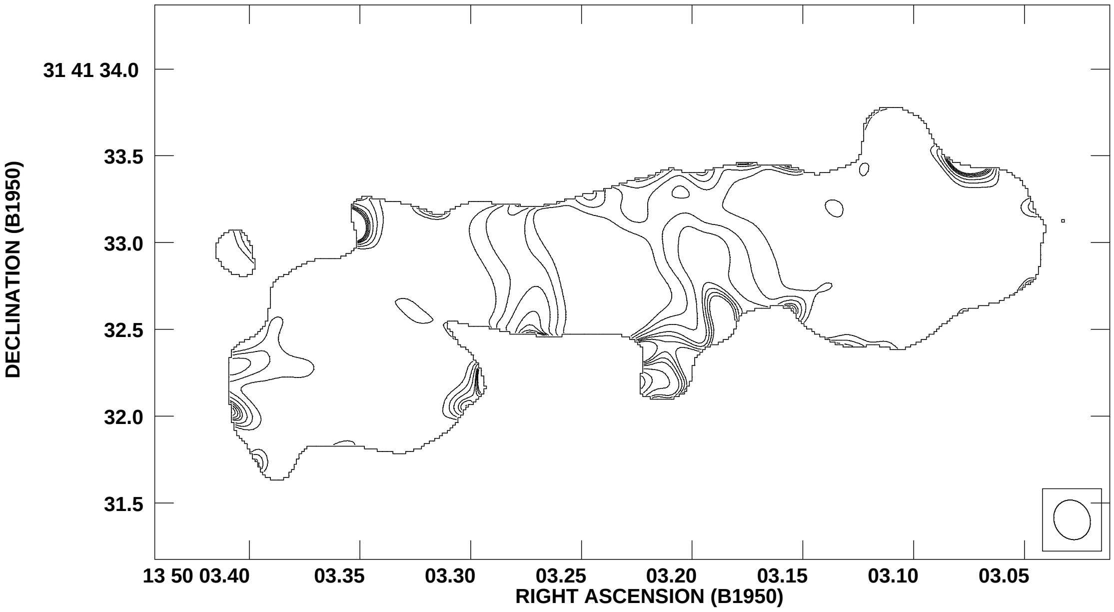

Figure 3.10: Spatial distribution of the narrow component of absorbing HI gas in 3C 293. The contour levels are τ equals 0.06, 0.1, 0.14, 0.18, 0.2, 0.22 and 0.24, the map is averaged optical depth over two channels centred at 13473.7 km s^{-1} and 13500 km s^{-1} and is coincident in velocity space with the narrow absorption component.

assume that the narrow HI absorbing component will have an extent approximately equal to that of the ionised gas component (radius ∼9-10 kpc). This in turn implies that the dust distributed in dust lanes is situated at a similar radius from the AGN as the narrow HI absorbing component and the ionised gas.

Schematically the distribution of the neutral gas and dust is shown in Fig. 3.11. This representation assumes that the ionised gas observed by van Breugel et al. (1984), the narrow HI absorbing component and dust lanes all exist at approximately the same radius from the central source. At this radius the velocity gradients observed will result from the rotation of the galaxy. Closer to the AGN, the more localised distribution of broad HI absorption and large velocity gradient infer a secondary distribution of gas within a kiloparsec of the AGN. This circumnuclear gas component, also observed in CO (Evans et al. 1999), can

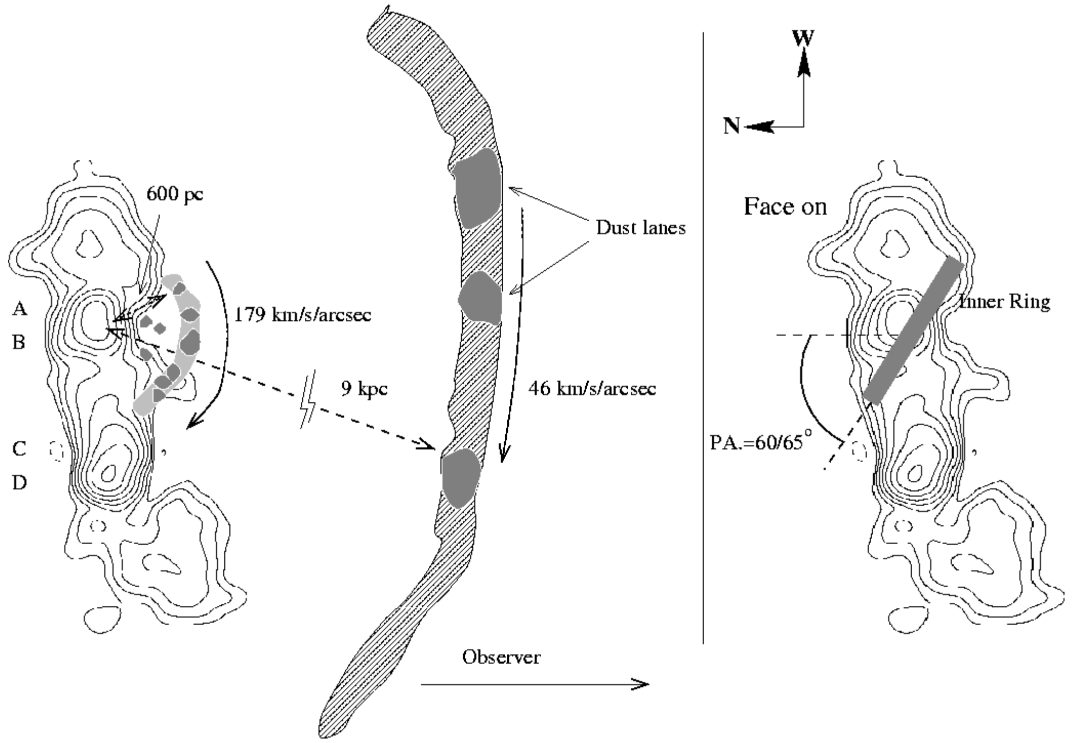

Figure 3.11: Schematic model of the spatial distribution of absorbing HI gas in 3C 293

be assumed to be compose of clumps of neutral gas rotating the AGN. Although the majority of the gas in this region lies along the observed velocity gradient, inferring a dominant rotational motion. There are also several components observed to be either blue- or redshifted with respect to the velocity gradient which maybe evidence of infall and outflow with respect to the AGN.

3.6 Conclusions

This chapter has presented the highest angular resolution observations of HI absorption, published to date, of the peculiar radio galaxy 3C 293[1]. These sub-

[1]Follow-up global VLBI HI observations of 3C 293 have now been made. Preliminary results from this experiment are presented in chapter 7.

arcsecond observations have allowed a detailed investigation into the neutral gas surrounding this radio source with linear scales as small as ~160 pc. At the 0.″2 resolution of MERLIN at 1.4 GHz the continuum of 3C 293 consists of a predominately east-west structure. This structure resolves into four luminous compact components along with a pair of more diffuse lobe-like structures, consistent with previous images made by Bridle et al. (1981) and Akujor et al. (1996).

Using both MERLIN and the GMRT neutral hydrogen is detected in absorption against the entire central region of this radio source. By direct comparison of the spatial extent of the HI optical depth and similar resolution broadband *HST* WFPC-2 images several bands of increased HI optical depth running approximately north-south which are coincident with areas of optical extinction, such as dust lanes, are found. In these areas the HI column densities are found to increase by approximately a factor of 4, compared to the rest of the source. The direct correlation of areas of high HI opacities with areas of high optical extinction has been seen against other similar radio sources notably 3C 305 (Cole 1999) where HI absorbing column densities of 1.9×10^{21} atoms cm^{-1} are observed against a limited part of the radio continuum which is obscured by a dust lane. By using galactic dust-to-gas ratios these HI column densities observed in 3C 293 have been used to an estimated optical extinction value of ~1.5 magnitudes for the dust lanes. This value is comparable to the optical extinction values seen in dust lanes of 3C 293.

Broad HI absorption has been observed against the western half of the radio source 3C 293. This absorption shows velocity gradient 179 $\mathrm{km\,s^{-1}\,arcsec^{-1}}$. This is interpreted as a edge-on ring of gas orientated at ~30° →45° to the radio axis and centred about the position of the active core within 3C 293 implying a dynamical mass of $\mathrm{M_{dyn}}(< 600\ \mathrm{pc}) \leq 3.9 \times 10^{9}(\sin^{-2} i)\ \mathrm{M_{\odot}}$.

In several other radio galaxies for example Hydra A (Dwarakanatha et al. 1995; Taylor 1996) and NGC 4261 (van Langevelde et al. 2000; Jaffe & McNamara

1994) H I absorption is believed to be the result of thin circumnuclear discs or tori. In both of these sources and in some Seyferts (e.g. NGC 4151, Mundell et al. 1995, Gallimore et al. 1999) H I discs are observed to exist on very small scales (<few 10s of parsecs) although this is not generally found, with most observed circumnuclear H I discs having scale sizes of $\sim$50$\rightarrow$100 pc (Gallimore et al. 1999). The circumnuclear disc that is observed in 3C 293 is large in comparison to those previously observed in radio galaxies although not considerably larger than those observed in many Seyfert galaxies. The existence of a disc of neutral gas in this highly distorted radio galaxy is consistent with orientation dependent unified schemes for AGN. The most probably fuelling mechanism for the active core being the result of infall from this reservoir of gas induced by galaxy-galaxy interactions in the recent history of 3C 293.